CrossMark

ORIGINAL PAPER

Electrochemical characterization of MWCNT/Ni(OH)$_2$ composites as cathode materials

M. G. Ortiz[1,2] · S. G. Real[1] · E. B. Castro[1]

Abstract The hydrothermal method was used to synthesize multi-walled carbon nanotube/nickel hydroxide composites (MWCNT/Ni(OH)$_2$). The structure and morphology of the prepared materials were characterized by X-ray diffraction and transmission electron microscopy. The electrochemical performance of cathodes prepared with multi-walled carbon nanotubes (MWCNT) loaded into the β-nickel hydroxide materials was investigated employing cyclic voltammetry, galvanostatic charge/discharge and electrochemical impedance spectroscopic measurements. It is shown that the cathode active material utilization increases for MWCNT/Ni(OH)$_2$ obtained after 24 h of hydrothermal synthesis. These composites exhibit a fairly good electrochemical performance as cathode materials. Based on the results, this fact could be associated with the formation of a continuous conductive network structure in the hydroxide matrix. The analyses of impedance data, according to a physicochemical model, allow the improvement of a better understanding of the main structural and physicochemical parameters that control the electrochemical performance of these systems.

Castro E.B. passed away on February 18, 2013.

✉ M. G. Ortiz
  mortiz@inifta.unlp.edu.ar

✉ S. G. Real
  sreal@inifta.unlp.edu.ar

1   Instituto de Investigaciones Fisicoquímicas Teóricas y Aplicadas (INIFTA), Facultad de Ciencias Exactas, Universidad Nacional de La Plata, C.C.16, Suc. 4 (1900), La Plata, Argentina

2   Centro de Investigación, Desarrollo en Ciencia y Tecnología de los Materiales (CITEMA), Facultad Regional La Plata, Universidad Tecnológica Nacional, Calle 60 y 124, La Plata, Argentina
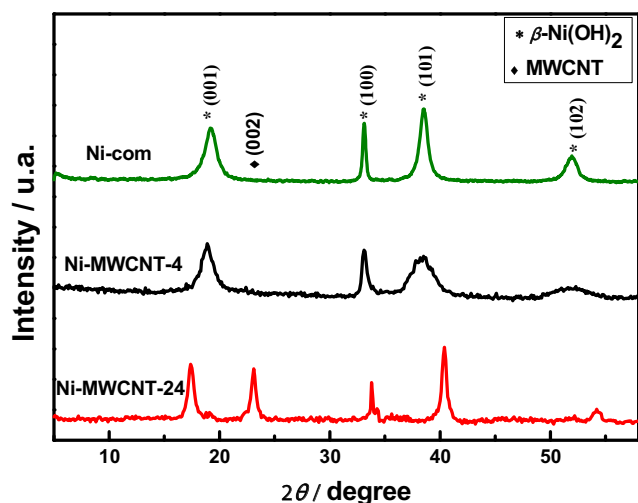
Introduction

The secondary nickel/metal hydride (Ni/MH) batteries are considered as ideally suited to a wide range of consumer applications, such as power tools and hybrid electric vehicles. These systems have good cyclability, high specific power and specific energy, as well as good safety in the medium term [1]. The capacity and cycle life of the cells are mainly determined by the properties of nickel hydroxide, the active material of positive electrodes [1, 2].

The electrode reaction can be expressed as follows:

$$Ni(OH)_2 + OH^- \rightleftarrows NiOOH + H_2O + e^-$$
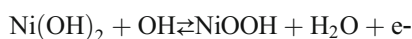
where the proton insertion occurs during discharge and vice versa during charge. The charge and discharge processes involve more than one phase, nickel hydroxide can be formed as α-Ni(OH)$_2$ and β-Ni(OH)$_2$; in the oxidation process, β-NiOOH or γ-NiOOH phases can be obtained [3–5]. In most cases, for rechargeable alkaline batteries, the active material of the positive electrode is β-Ni(OH)$_2$. Although α-Ni(OH)$_2$ exhibits superior electrochemical properties than that of β-Ni(OH)$_2$, it is unstable in alkaline media and can easily be converted to β-Ni(OH)$_2$ [6]. γ-NiOOH species can also be formed under conditions of overcharging or high rate charging. The conversion of β-NiOOH to γ-NiOOH is accompanied by a large volumetric change and this process may result in the swelling of the nickel electrode. Consequently, the formation of γ-NiOOH considerably damages the nickel electrode and induces a rapid capacity deterioration during cell cycling [3].
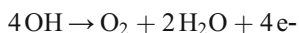
 Springer

Fig. 1 XRD patterns of commercial nickel hydroxide and synthesized composites

The oxygen evolution reaction can also occur during the operation of the nickel electrodes:

$$4\,OH \rightarrow O_2 + 2\,H_2O + 4\,e\text{-}$$

The generated gas can cause an excessive pressure build-up during charge and overcharge. This gassing process strongly affects the performance and life of Ni-MH batteries [1–6].

The performance of nickel hydroxide, as active material in positive electrodes, is affected by its poor electronic conductivity due to the *p*-type semiconductor nature [2]. Significant efforts have been devoted to develop new electrode materials for improving the electrochemical performance of Ni(OH)$_2$. The proposals to enhance Ni(OH)$_2$ properties include: nanostructured and microstructured control of Ni(OH)$_2$ through the modification of synthesis parameters [7–10], stabilization of α-Ni(OH)$_2$ by incorporating Al [11–13], modification of the electrode surface by electroless deposition [14–16], the use of different supports [17], the change of binding materials [18] and the incorporation of additives (Co, Ca Ba, Fe, Zn and carbon materials) using different methods [19–27]. Particularly, carbon nanotubes (CNT) have been studied as additives since they have high electrical conductivity, excellent mechanical properties, good bending strength, accessible surface area, low resistance and high stability. Consequently, CNT are considered to be suitable materials for different energy storage/conversion systems [2, 28, 29].

In this paper, MWCNT/Ni(OH)$_2$ composites were synthesized by the hydrothermal method at different times (4 and 24 h). These two hydrothermal periods were selected considering that they are responsible for the main differences in the obtained morphologies and structures of the nanoscale nickel hydroxide materials [9, 30, 31]. These samples were characterized by X-ray diffraction (XRD) and transmission electron microscopy (TEM), and the electrochemical performance of

Fig. 2 TEM images of **a** MWCNT/Ni-4 composites and **b** MWCNT/Ni-24 composites
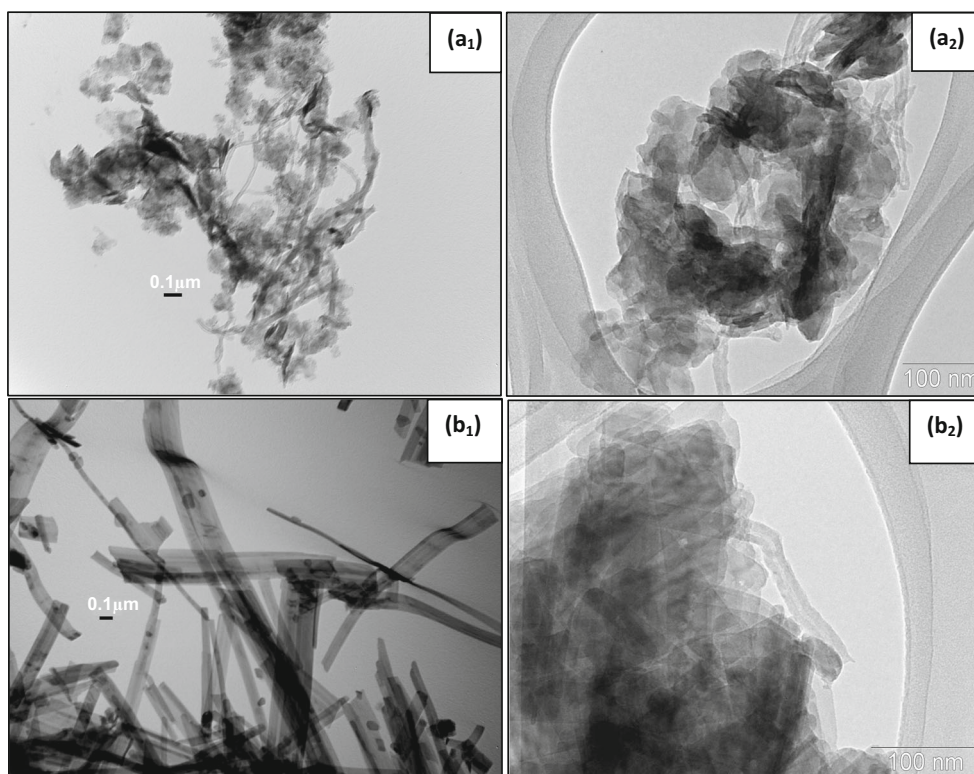
these products, as active material for positive electrodes, was investigated employing cycling voltammetry (CV), charge–discharge and electrochemical impedance spectroscopy (EIS) techniques.

In this work, the EIS results of the MWCNT/ Ni(OH)$_2$ samples as well as those prepared with commercial nickel hydroxide were analysed employing a physicochemical model, previously developed in the laboratory [32–35], to investigate and to enhace the understanding of the main structural and physicochemical parameters that control the electrochemical performance of these systems. Although the electrochemical behaviour of these electrode materials has been previously studied [2, 29], it is considered that there has been no attempt to model EIS results in this fashion.

Experimental

Materials preparation

All the chemical reagents used in this study were of analytical grade. In a typical procedure, 0.098 g MWCNT (Aldrich), 20 ml of 0.8 M Ni(SO$_4$) (Mallinckrodt, 99.8 wt.%) aqueous solutions and 20 ml of 1.6 M NaOH (Anedra, 98.6 wt.%) were mixed with vigorous stirring. The mixed reactants were hydrothermally treated at 180 °C for 4 and 24 h in a Teflon-lined autoclave. After this procedure, the samples were cooled to room temperature and the green precipitates were filtered, washed with distiller water and dried at 70 °C for 24 h. Two kinds of MWCNT/Ni(OH)$_2$ composites were obtained and they were called MWCNT/Ni-4 and MWCNT/Ni-24.

Fig. 3 SEM micrographs for E-Ni-com samples **a** ×1,000 and **b** ×8,000, E-MWCNT/Ni-4 samples **c** ×1,000 and **d** ×8,000 and E-MWCNT/Ni-24 samples **e** ×1,000 and **f** ×8,000
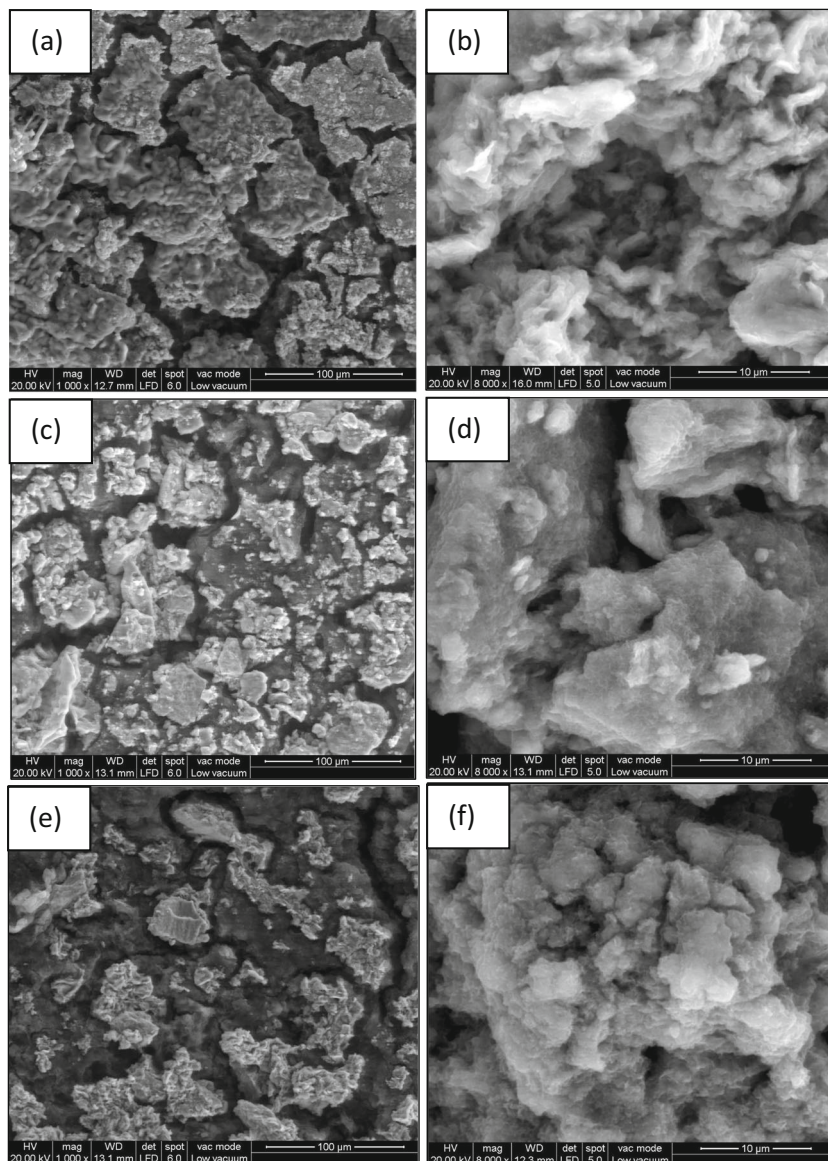
Pasted nickel electrodes (E-Ni-com, E-MWCNT/Ni-4 and E-MWCNT/Ni-24) were prepared as follows: 65 wt.% commercial $Ni(OH)_2$ (Aldrich) or $MWCNT/Ni(OH)_2$ composites were mixed with 35 wt.% teflonized carbon black (Vulcan XC-72, with 30 wt.% polytetrafluoroethylene). The mixtures were pressed onto a nickel form substrate under a pressure of 300 kg cm^{-2}. The area of electrodes was 0.4 cm^{-2} with a thickness of 0.075 cm.

Structural and electrochemical characterization

The phase and crystallinity of the products were characterized using PW-1730 Philips X-ray diffractometer ($\lambda = 1.54178$ Å, $5° < 2\theta d < 58°$). The morphology and crystal structures of the synthesized samples were analysed by transmission electron microscopy (TEM, JEM 1200EX II model, Jeol).

Electrochemical measurements were carried out in a three-compartment cell, with the corresponding working (nickel electrode), counter (nickel mesh of large specific area) and reference (Hg/HgO_{ss}) electrodes, employing 7 M KOH solutions at 30 °C as electrolyte.

Voltammograms were obtained at scan rates of 1 mV s^{-1}, between 0.05 and 0.55 V; charge–discharge curves were run at different current densities up to 0.55 V cut-off voltage. EIS measurements were performed under potentiostatic control using a frequency response analyser Solartron 1250 coupled to a potentiostat EG&G model PAR 273. EIS measurements were conducted over a 65 kHz to 19 mHz frequency range and under equilibrium conditions by employing a sinusoidal perturbation signal of small amplitude (5 mV).

The surface structure of the electrodes was studied using scanning electron microscopy (SEM). The SEM images were
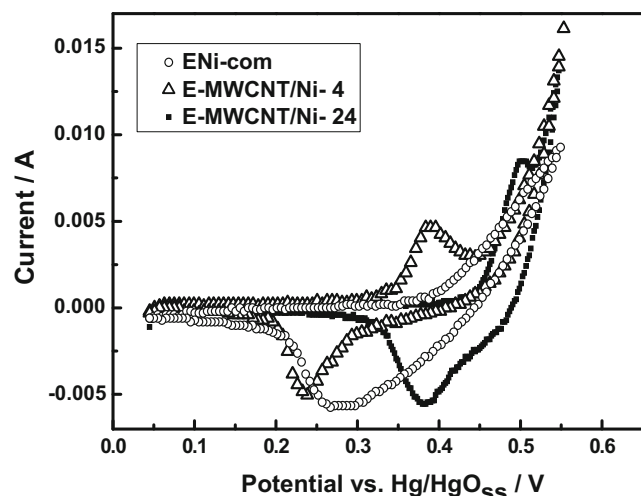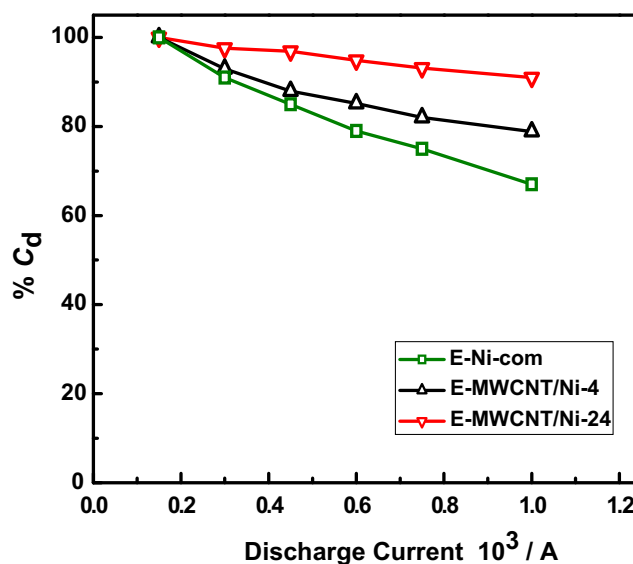

Fig. 5 Percentage of discharge capacity related to the maximum capacity (% C_d) vs. discharge current

obtained employing a scanning electron microscope Philips SEM model 505 with an image digitizer System Soft Imaging ADDA II. The experiments to perform the electrochemical and structural characterization were repeated at least three times in order to assure reproducibility.

Results and discussion

Microstructure and morphology studies of composites

The phases of the synthesized composites were identified by X-ray diffraction (Fig. 1). It can be seen that the diffraction peaks of all samples are indexed as the hexagonal phase of typical β-nickel hydroxide (JCPDS-14-0117). Compared with Ni-com and MWCNT/Ni-24, the diffraction peaks of MWCNT/Ni-4 are noticeably broadened, indicating either poor crystallinity or smaller crystalline size. These facts can be attributed to the increased crystal defects due to the existence of stack faults and to the presence of other polymorphic modifications such as interstratified phases [26]. A diffraction peak at $2\theta = 24°$ (MWCNT/Ni-24 composite) can be indexed to the (002) plane of MWCNT, corresponding

Fig. 4 CV curves of E-Ni-com, E-MWCNT/Ni-4 and E-MWCNT/Ni-24 electrodes

Table 1 Potential peak values from CV features

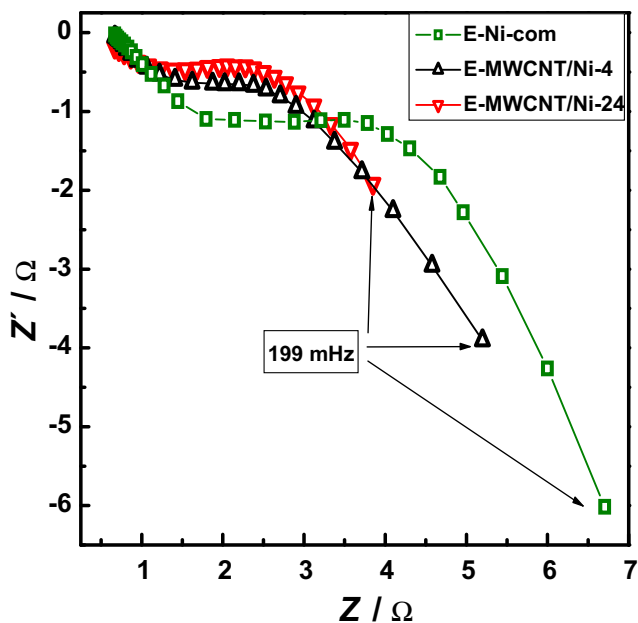| Working electrodes	E_a [V]	E_c [V]	$\Delta E_{a,c}$ [V]	E_O [V]
E-Ni-com	≈0.500	0.270	0.230	<0.500
E-MWCNT/Ni-4	0.394	0.240	0.154	0.500
E-MWCNT/Ni-24	0.499	0.385	0.114	>>0.500

Fig. 6 Experimental Nyquist plots of E-Ni-com, E-MWCNT/Ni-4 and E-MWCNT/Ni-24 electrodes

to the P63/mmc space group slightly shifted towards smaller 2θ values [36]. No peaks corresponding to impurities were observed.

The morphology of synthesized composites was observed by TEM (Fig. 2). TEM images show that the composites are formed by agglomeration of nickel hydroxide structures where the MWCNT material appears to be distributed among them. The composite structures exhibit significant morphological changes according to the hydrothermal synthesis time. In Fig. 2 (a₁, b₁), it can be observed that when the reaction time is 24 h, the composite products appear to have a longitudinal growth and show ribbon morphology.

Electrode surface characterization

The information about electrode surface topography was analysed by SEM. In Figs. 3, 4 and 5 (at ×1,000 and ×8, 000), it can be seen that the electrodes show a very similar porous structure with defined holes or pores.

Electrochemical properties

The stabilized voltammograms corresponding to pasted nickel electrodes, after 12 cycles, are shown in Fig. 4. The voltammogram peaks (anodic peak potentials, E_a, and cathodic peak potentials, E_c) associated with the redox reaction $Ni(OH)_2/NiOOH$ are observed. In addition, it can be seen that, for the electrodes with MWCNT/Ni composites, oxidation peak potentials (E_a) are separated from those corresponding to the oxygen evolution reaction (E_O). However, the CV curve related to E-Ni-com electrodes shows that at a potential of around 0.5 V, the nickel hydroxide process overlaps with the oxygen evolution reaction. The data derived from cyclic voltammetry results (Fig. 4) are listed in Table 1. The difference between the anodic and cathodic peak positions ($\Delta E_{a,c}$) is taken as the reversibility estimation of the redox reaction. The cathodic and anodic peak potentials of E-MWCNT/Ni-4 electrodes are shifted to more negative values than those corresponding to E-MWCNT/Ni-24 electrodes. However, a better reversibility related to the redox process is observed in the CV of E-MWCNT/Ni-24 electrodes.

Figure 5 exhibits the percentage of the discharge capacity, related to the maximum capacity (%C_d), as a function of the discharge current. The plot shows that at very low discharge current values, the rate-capability behaviour of the studied samples is fairly similar. However, for increasing discharge current requirements, the E-MWCNT/Ni-24 electrodes show
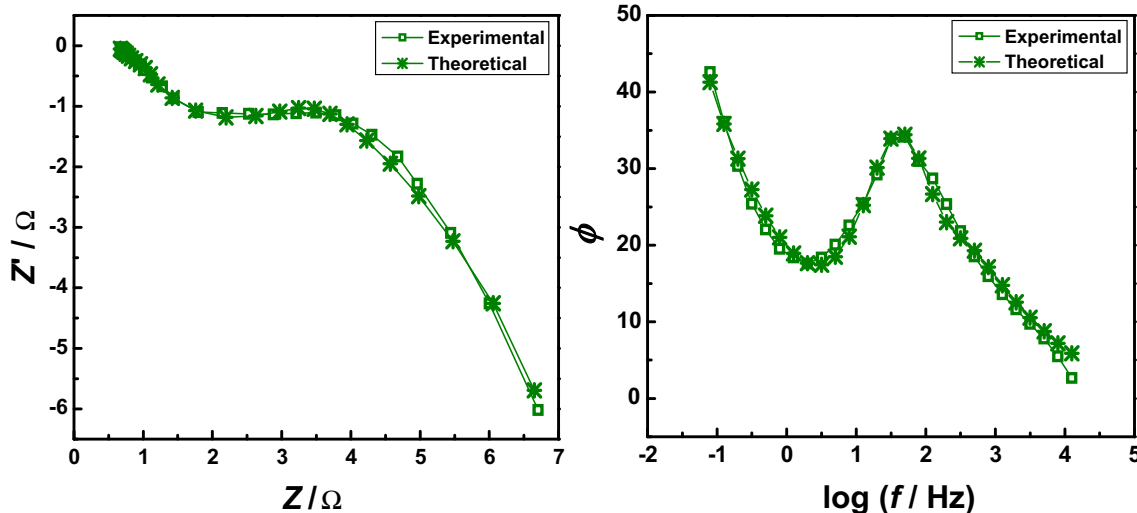

Fig. 7 Experimental and theoretical impedance plots for E-Ni-com electrodes
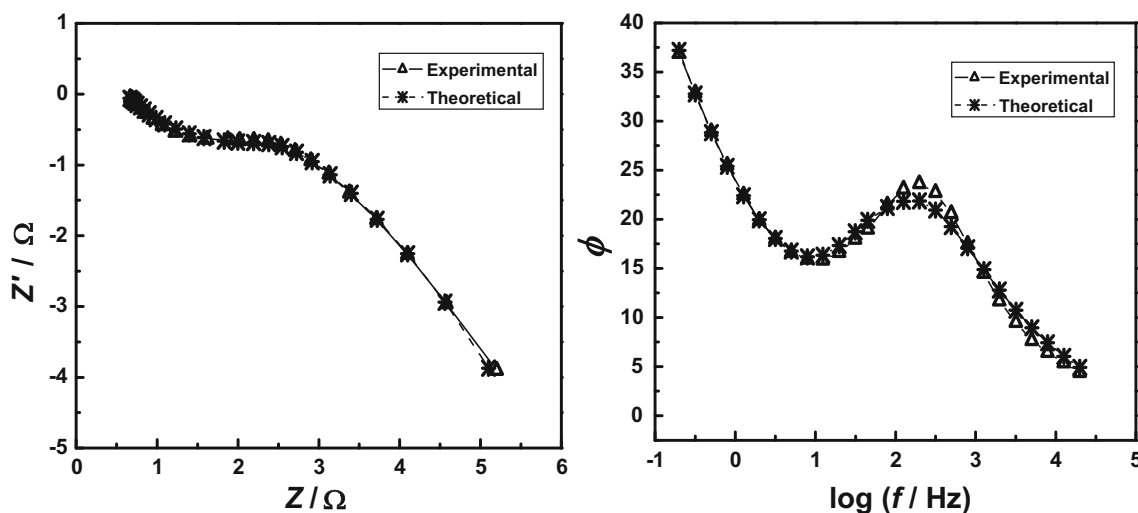
Fig. 8 Experimental and theoretical impedance plots for E-MWCNT/Ni-4 electrodes

that their kinetics is faster than that corresponding to E-MWCNT/Ni-4 and E-Ni-com electrodes (up to 20 and 26 % higher, respectively).

Impedance measurements were also carried out to study the electrochemical performance of nickel electrodes. Figure 6 exhibits the typical experimental Nyquist plots of E-Ni-com, E-MWCNT/Ni-4 and E-MWCNT/Ni-24 samples at 75 % of state of discharge (SOD).

Impedance spectra of the studied samples exhibit the same general features. Figure 6 shows, at high frequencies, a linear behaviour with a slope of approximately 45° related to the porosity of the electrode; at intermediate frequencies a semicircle that corresponds to the charge transfer resistance and, in the low frequency interval, a time constant characteristic of diffusional processes.

Experimental impedance data were fitted in terms of a model that has been described in previous publications

[32–35]. The transfer function derived from this model describes the nickel hydroxide electrode as a flooded porous structure where the charge–discharge electrochemical process takes place at the active material/electrolyte interface, this being coupled to proton diffusion in the active material.

According to this model, the theoretical impedance of the system is described by the impedance of the porous electrode per unit geometric area (Zp):

$$Z_p(j\omega) = \frac{L}{A_p(K+\sigma)}\left[1 + \frac{2 + \left(\frac{\sigma}{K}+\frac{K}{\sigma}\right)\cosh v(j\omega)}{v(j\omega)\sinh v(j\omega)}\right]$$

where

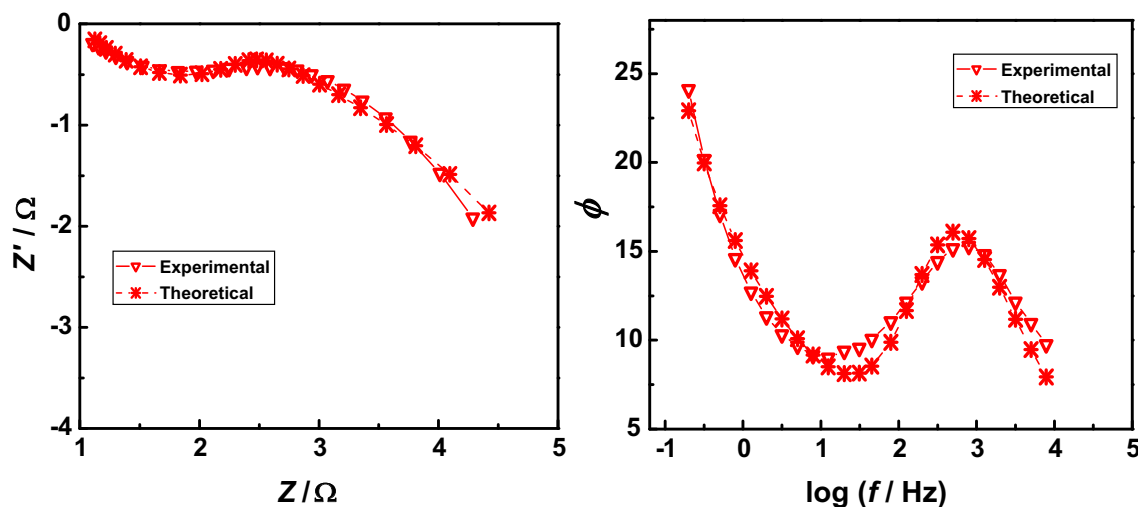$$v(j\omega) = L\left(\frac{K+\sigma}{K\sigma}\right)^{1/2} Z_i^{-1/2}(j\omega)$$

Fig. 9 Experimental and theoretical impedance plots for E-MWCNT/Ni-24 electrodes

Table 2 Parameters derived from the fitting procedure

Working electrodes	SOD	C_{dl} [F cm^{-3}]	k [Ω^{-1} cm^{-1}]	σ [Ω^{-1} cm^{-1}]	i_o [A cm^{-2}]	D [cm^2 s^{-1}]
E-Ni-com	75	0.05 (±0.01)	0.06	0.3 (±0.1)	1.3 (±0.4) 10^{-3}	1.96 (±0.03)10^{-12}
E-MWCNT/Ni-4	75	0.09 (±0.01)	0.06	18.2 (±0.1)	1.5 (±0.4)10^{-3}	3.21(±0.03)10^{-12}
E-MWCNT/Ni-24	75	0.12 (±0.01)	0.06	29.5 (±0.1)	2.0 (±0.4)10^{-3}	4.55 (±0.03)10^{-12}

L being the electrode thickness, A_p the electrode geometric area (cross section), κ and σ the effective conductivities of the liquid and solid phases, respectively, and Z_i the impedance of the solid /liquid interface per electrode unit volume (Ω cm^3). The interfacial impedance (Z_i) is derived considering the double layer capacitance impedance (Z_{dl}) linked in parallel with the faradaic reaction impedance (Z_F). According to the physicochemical model [32–35], Z_F is represented by a Warburg-type impedance as:

$$Z_F(j\omega) = \frac{R_T}{a_a} + \frac{A}{a_a\sqrt{j\omega}} = \frac{RT}{i^o F a_a} + \frac{RT}{F^2 SOD(1-SOD)c_m a_a \sqrt{D}\sqrt{j\omega}}$$

where SOD accounts for the state of discharge of the electrode, a_a is the active area per unit volume, c_m corresponds to the maximum admitted proton concentration, i_o is the exchange current density, and D is the proton diffusion coefficient. The fitting programme was developed based on the Nelder-Meade simplex search algorithm, included in the Matlab package, in order to perform parameter identifications. During the fitting procedure, the objective function to be minimized was the cost function J_p, defined as:

$$J_p = \frac{1}{K}\sum_k Ie(p,\omega_k)I^2 = \frac{1}{K}\sum_k I\frac{Z_e(\omega_k)-Z_p(p,\omega_k)}{Z_e(\omega_k)}I^2$$

where K is the number of experimental frequencies (ω), and Z_e and Z_P the experimental and theoretical impedance values corresponding to the frequency ω_k. This algorithm returns a parameter vector [p] that is a local minimizer of J_p, near the starting vector [po]. The fitting was considered acceptable when $J_p < 5.10^{-3}$.

Accordingly, a good agreement between experimental and theoretical impedance data can be observed in Figs. 7, 8 and 9.

The characteristic parameters derived from the fitting procedure along with the corresponding errors generated by the fitting condition of $J_p < 5.10^{-3}$, are listed in Table 2 for a constant SOD: the double layer capacitance per unit volume (C_{dl}), the effective conductivity of the solid phase (σ), the exchange current density (i_o) and the diffusion coefficient (D). The effective electrolyte conductivity value (κ) was taken as equal to 0.06 Ω^{-1} cm^{-1}. Taking into account SEM results, a similar porosity of about 20 % was considered for the fitting procedure, this being a porosity factor contained in the κ value [35].

The results in Table 2 show that E-MWCNT/Ni-24 electrodes present the largest C_{dl} and σ values. However, i_o and D values appear to be of the same order of magnitude for all the studied electrodes and they are comparable to those described in the literature [37–39]. The errors generated by the fitting procedure for each parameter are included in Table 2.

Considering all the results, greater reversibility of the redox process Ni(OH)$_2$/NiOOH and better rate capability responses were obtained with E-MWCNT/Ni-24 electrodes. The superior electrochemical performance of these electrodes could be related to their lower electrochemical impedance.

According to the estimated characteristic parameters, derived from the physicochemical model, the improvement in the electrochemical behaviour of E-MWCNT/Ni-24 electrodes can be attributed to their higher C_{dl} and σ values (Table 2). Taking into consideration TEM results for 24 h hydrothermal synthesis (Fig. 2 (a$_1$–b$_1$)), these facts can probably be related to the preferential longitudinal growth of products, with ribbon morphology, that allow improving a continuous conductive network structure in the hydroxide matrix.

Conclusions

In summary, carbon nanotubes were used as a functional additive to improve the electrochemical performance of pasted nickel electrodes. The MWCNT/Ni(OH)$_2$ composites were prepared by a simple hydrothermal method (employing 4 and 24 h of synthesis time) and characterized by XRD, SEM and TEM techniques. The synthesized materials were identified by XRD as β-Ni(OH)$_2$ and the composite structure was characterized by TEM experiments. These studies showed that the MWCNT allow improving the network within the Ni(OH)$_2$ structure.

Commercial Ni(OH)$_2$ and MWCNT/Ni(OH)$_2$ composites were used as active material of the nickel electrodes, and their electrochemical properties were evaluated by CV, charge–discharge curves and EIS measurements. These results indicate that the addition of MWCNT to the active material improves the operating performance of these electrodes. It was shown that longer hydrothermal synthesis times (24 h) lead to the formation of materials with superior electrochemical performance, reversibility, material utilization and specific discharge capacity. These facts can possibly be attributed to a better connection among particles themselves and a structure that improve the whole electron conductive network of the electrode. It can be concluded that according to the parameters

derived from the physicochemical model, the improvement in active material utilization observed for E-MWCNT/Ni-24 electrodes could be related to their higher C_{dl} and σ values.

References

1. Zhang W, Jiang W, Yu L, Zhongzhen F, Xia W, Yang M (2009) Int J Hydrog Energy 34:473–480
2. Lv J, Tu JP, Zhang WK, Wu JB, Wu HM, Zhang B (2004) J Power Sources 132:282–287
3. Snook Graeme A, Duffy Noel W, Pandolfo Anthony G (2007) J Power Sources 168:513–521
4. Van der Ven A, Morgan D, Meng YS, Ceder G (2006) J Electrochem Soc 153(2):A210–A215
5. Shukla AK, Venugopalan S, Hariprakash B (2001) J Power Sources 100:125–148
6. Ren J, Zhou Z, Gao XP, Yan J (2006) Electrochim Acta 52:1120–1126
7. Liu X, Yu L (2004) J Power Sources 128:326–330
8. Wang X, Sebastian PJ, Millan A-C, Parkhutik PV, Gamboa SA (2005) J New Mat Electr Syst 8:101–108
9. Xiao-yan G, Deng J-c (2007) Mater Lett 61:621–625
10. Wang X, Luo H, Parkhutik PV, Millan A-C, Matveeva E (2003) J Power Sources 115:153–160
11. Bing L, Huatang Y, Yunshi Z, Zuoxiang Z, Deying S (1999) J Power Sources 79:277–280
12. Liu B, Yuan H, Zhang Y (2004) Int J Hydrog Energy 29:453–458
13. Dai J, Li SFY, Xiao TD, Wang DM, Reisner DE (2000) J Power Sources 89:40–45
14. Wang X, Luo H, Yang H, Sebastian PJ, Gamboa SA (2004) Int J Hydrog Energy 29:967–972
15. Wang X, Yan J, Yuan H, Zhou Z, Song D, Zhang Y, Zhu L (1998) J Power Sources 72:221–225
16. Ortiz MG, Castro EB, Real SG (2014) Int J Hydrog Energy 39:6006–6012
17. Ramesh TN, Jayashree RS, Kamath PV, Rodrigues S, Shukla AK (2002) J Power Sources 104:295–298
18. Fukunaga H, Kishimi M, Igarashi N, Ozaki T, Sakai T (2005) J Electrochem Soc 152(1):A42–A46
19. Begum SN, Muralidharan VS, Ahmed BC (2009) Int J Hydrog Energy 34:1548–1555
20. Marcio V, Salvador RP, Córdoba de Torresi SI (2009) Ultrason Sonochem 16:35–40
21. Ortiz MG, Real SG, Castro EB (2014) Int J Hydrog Energy 39:8661–8666
22. Provazi K, Giz MJ, Dall'Antonia LH, Córdoba de Torresi SI (2001) J Power Sources 102:224–232
23. Yuan A, Cheng S, Zhang J, Cao C (1998) J Power Sources 76:36–40
24. Cheng S, Anbao Y, Hong L, Jianqing Z, Chunan C (1998) J Power Sources 76:215–217
25. Krejčí I, Mrha J, Folkesson B, Larsson R (1987) J Power Sources 21:77–90
26. Zhang WK, Xia XH, Huang H, Gan YP, Wu JB, Tu JP (2008) J Power Sources 184:646–651
27. Sierczynska A, Lota K, Lota G (2010) J Power Sources 195:7511–7516
28. Gooding JJ (2005) Electrochim Acta 50:3049–3060
29. Song QS, Aravindaraj GK, Sultana H, Chan SLI (2007) Electrochim Acta 53:1890–1896
30. Jiao Q-Z, Tian Z-L, Zhao Y (2007) J Nanopart Res 9:519–522
31. Yan D, Wang R, Zhang J, Liu Z (2004) J Phys Chem B 108:23:7531–7533
32. Ortiz MG, Castro EB, Real SG (2012) Int J Hydrog Energy 37:10365–10370
33. De Levie R (1967) In: Delahay P (ed) Advances in electrochemistry and electrochemistry engineering, vol 6. Interscience, NY, pp 329–361
34. Castro EB, Cuscueta DJ, Milocco RH, Ghilarducci AA, Salva HR (2010) Int J Hydrog Energy 35:5991–5998
35. Ortiz M, Becker D, Garaventta G, Visintin A, Castro EB, Real SG (2011) Electrochim Acta 56:7946–7954
36. Li J, Liu E-h, Li W, Meng X-y, Tan S-t (2009) J Alloys Comp 478:371–374
37. Paxton B, Newman J (1997) J Electrochem Soc 144:3818–3831
38. Zhang C, Su-Moon P (1987) J Electrochem Soc 134:2966–2970
39. Mao Z, De Vidts P, White RE, Newman J (1994) J Electrochem Soc 141:54–64